Solution Conformation of [AF]dG Opposite a −2 Deletion Site in a DNA Duplex: Intercalation of the Covalently Attached Aminofluorene Ring into the Helix with Base Displacement of the C^8-Modified *syn* Guanine and Adjacent Unpaired 3′-Adenine into the Major Groove†

Bing Mao,‡ Brian E. Hingerty,§ Suse Broyde,|| and Dinshaw J. Patel*,‡

Cellular Biochemistry and Biophysics Program, Memorial Sloan-Kettering Cancer Center, New York, New York 10021, Health Sciences Research Division, Oak Ridge National Laboratory, Oak Ridge, Tennessee 37831, and Biology Department, New York University, New York, New York 10003

Received July 13, 1995; Revised Manuscript Received October 27, 1995®

ABSTRACT: This paper reports the solution conformation of the covalent aminofluorene-C^8-deoxyguanosine [AF]dG adduct positioned opposite a −2 deletion site in a DNA oligomer duplex. The combined NMR and molecular mechanics computational studies were undertaken on the [AF]dG adduct embedded in the d(C5-[AF]G6-A7-C8)·d(G17-G18) sequence context in a duplex containing 12 residues on the modified strand and 10 on the partner strand, with no bases opposite the [AF]dG6−dA7 segment. The exchangeable and nonexchangeable protons of the aminofluorene moiety and the nucleic acid were assigned following analysis of two-dimensional NMR data sets in H_2O and D_2O solution. The solution conformation of the [AF]dG·2del 12-mer duplex has been determined by incorporating intramolecular and intermolecular proton−proton distances defined by upper and lower bounds deduced from NOESY spectra as restraints in molecular mechanics computations in torsion angle space. The aminofluorene ring of [AF]dG6 is intercalated between intact Waston−Crick dC5·dG18 and dC8·dG17 base pairs with the deoxyguanosine base of [AF]dG6 in a *syn* alignment displaced into the major groove. The *syn* glycosidic torsion angle at [AF]dG6 is supported by both carbon and proton chemical shift data for the sugar resonances of the modified deoxyguanosine residue. The unpaired dA7 base is also looped out of the helix into the major groove with the purine rings of [AF]dG6 and dA7 stacking on each other in the groove. The long axis of the intercalated aminofluorene ring is parallel to the long axis of the flanking dG·dC base pairs. The intercalation site is wedge shaped with a pronounced propeller-twisting and buckling of the dC5·dG18 base pair. The deoxyguanosine base of [AF]dG6, which is positioned in the major groove, is inclined relative to the helix axis and stacks over the 5′-flanking dC5 residue in the solution structure. The intercalative base displacement structure of the [AF]dG·2del 12-mer duplex exhibits several unusually shifted proton resonances that can be readily accounted for by the ring current contributions of the deoxyguanosine purine and carcinogen fluorene aromatic rings of the [AF]dG6 adduct. We note similarities between the present conformation of [AF]dG positioned opposite a −2 deletion site with our earlier conformational studies of [AF]dG positioned opposite a −1 deletion site [Mao, B., Cosman, M., Hingerty, B. E., Broyde, S., & Patel, D. J. (1995) *Biochemistry 34,* 6226−6238]. For both conformations, the aminofluorene carcinogen inserts into the helix at the deletion site through base displacement of the modified deoxyguanosine in a *syn* alignment into the major groove and directed toward its 5′-neighbor in the sequence. These structures provide a molecular explanation of how transient strand slippage of the lesion-containing segment can be accommodated by a double helix following translesion synthesis.

The carcinogen 2-aminofluorene (AF) has been under intensive investigation as a model compound for carcinogenesis by aromatic amines for over 50 years. It was originally synthesized as a potential insecticide but was not put to use once animal studies revealed its carcinogenicity. Aromatic amines are representative of a large category of chemical carcinogens that are present widely in the environment, in tobacco smoke, automobile exhaust, and barbecued meat. The goal of understanding the mechanisms responsible for their carcinogenic effect has driven the decades-long efforts, which have been recently reviewed by Heflich and Neft (1994).

Chemically or metabolically activated 2-aminofluorene reacts with DNA both *in vitro* and *in vivo* to form an adduct to C^8 of guanine (**1**) [reviewed in Beland and Kadlubar (1990)]. Mutational consequences due to or ascribed to this adduct [reviewed in Haflich and Neft (1994)] have been investigated in a number of *in vitro* and *in vivo* systems, both bacterial and mammalian (Bichara & Fuchs, 1985; Mah et al., 1991; Sahm et al., 1989; Michaels et al., 1991; Carothers et al., 1993; Shibutani & Grollman, 1993; Tebbs

† This research is supported by NIH Grant CA-49982 to D.J.P., by NIH Grant CA-28038, NIH Grant RR-06458, and DOE Grant DE-FG02-90ER60931 to S.B., and by DOE Contract DE-AC05-840R21400 with Martin-Marietta Energy Systems and DOE OHER Field Work Proposal ERKP931 to B.E.H.

‡ Memorial Sloan-Kettering Cancer Center.
§ Oak Ridge National Laboratory.
|| New York University.

® Abstract published in *Advance ACS Abstracts,* December 15, 1995.

0006-2960/95/0434-16641$09.00/0

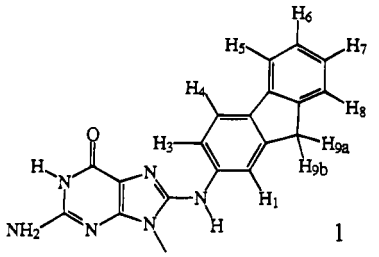

1

& Romano, 1994; Melchior et al., 1994; Shelton & DeMarini, 1995). The bulk of the data indicate generation of AF-induced point mutations, especially dG·dC to dT·dA transversions, but −1 and −2 deletions are also observed and could well be important in specific sequence contexts.

In the present work we present the solution conformation of an [AF]dG adduct opposite a −2 deletion site. This is, to our knowledge, the first molecular view in solution of any polycyclic aromatic hydrocarbon or amine adduct to DNA in a −2 deletion context, and it reveals the stabilizing interactions that permit such conformations to form. Moreover, the conformation shares features of base displacement and carcinogen−base stacking with our previously determined solution conformation of an [AF]dG adduct opposite a −1 deletion site (Mao et al., 1995) and (+)-*trans-anti*- and (+)-*cis-anti*-benzo[*a*]pyrenediol epoxide (BPDE) adducts to N^2 of deoxyguanosine positioned opposite −1 deletion sites (Cosman et al., 1994a,b) as well as with our recently determined solution conformation of a (+)-*trans-anti*-BPDE adduct at a single strand−duplex junction that models an arm of a replication fork (Cosman et al., 1995). These results suggest that such forms could represent mutagenic conformers irrespective of the specific polycyclic aromatic moiety or the linkage site to DNA.

MATERIALS AND METHODS

Oligonucleotide Synthesis. The deoxyoligonucleotides d(C-C-A-T-C-G-A-C-T-A-C-C) and d(G-G-T-A-G-G-A-T-G-G) were synthesized on an Applied Biosystems model 392 DNA synthesizer and purified by reverse-phase HPLC.

Preparation of Adduct. The d(C-C-A-T-C-G-A-C-T-A-C-C) sequence was converted into the d(C-C-A-T-C-[AF]G-A-C-T-A-C-C) adduct sequence as described previously (Norman et al., 1989). The d(C-C-A-T-C-[AF]G-A-C-T-A-C-C) 12-mer strand was annealed with the complementary d(G-G-T-A-G-G-A-T-G-G) 10-mer strand at 70 °C, and the stoichiometry was followed by monitoring single-proton resonances in both strands.

Sample Preparation. The NMR spectra of the [AF]-dG·2del 12-mer duplex (3 mM in duplex) and the corresponding control dG·2del 12-mer duplex (3 mM in duplex) were recorded in 0.1 M NaCl, 10 mM phosphate, 1 mM EDTA solution containing either D_2O or 90:10 H_2O/D_2O (v/v). All NMR spectra were recorded on samples at pH 7.0.

Optical Melting Experiments. UV melting assays were performed using a HP 8452A diode array spectrophotometer interfaced with an HP 89090A Peltier temperature control unit. The control dG·2del 12-mer and the [AF]dG·2del 12-mer duplexes (strand concentration 10 μM) were dissolved in 20 mM phosphate buffer containing 0.1 M NaCl and 1 mM EDTA at pH 7.0. The order−disorder transition was monitored at 260 nm with a heating rate of 1 °C per minute. The temperature range was 10−70 °C.

NMR Experiments. All NMR data sets were recorded on Varian Unity Plus 500 and 600 MHz NMR spectrometers. A combination of through-space nuclear Overhauser effect (NOESY) and through-bond-correlated (COSY, TOCSY) two-dimensional spectra were recorded and analyzed to assign the aminofluorene and nucleic acid protons in the [AF]dG·2del 12-mer duplex. NOESY data sets on the modified duplex spectra in H_2O buffer were collected with 100 and 150 ms mixing times at 1 °C using an optimized jump−return pulse sequence for solvent suppression. The corresponding NOESY spectra in D_2O buffer were collected with mixing times of 50, 70, 100, 150, 200, and 300 ms at 25 °C. The through-bond TOCSY spectra were recorded in D_2O buffer at spin lock times of 40 and 80 ms at 25 °C.

The indirect detected proton−phosphorus correlation spectrum was recorded on the [AF]dG·2del 12-mer duplex in D_2O at 25 °C using the pulse sequence described by Sklenar et al. (1986). Both proton and phosphorus sweep widths were set to 6 ppm with a 1.3 s presaturation of the residual HOD resonance. The phosphorus spectra were referenced relative to external 10% trimethylphosphate (TMP).

A proton−carbon HMQC correlation spectra on the [AF]dG·2del 12-mer duplex was recorded in D_2O buffer at 25 °C. The proton carrier frequency was set to 4.5 ppm with a sweep width of 8.5 ppm, while the ^{13}C carrier frequency was set to 67.0 ppm with a sweep width of 66.0 ppm. The carbon spectra were referenced relative to external 3-(trimethylsilyl)propionate (TSP) using the method described by Bax and Subramanian (1986).

The volume integrals of NOE cross-peaks as a function of four mixing times (50, 70, 100, and 150 ms) were measured to generate the build-up curves for nonexchangeable protons in D_2O solution. The interproton distances were calculated based on the two-spin approximation using the dT(NH3)−dA(H2) fixed distance of 2.92 Å for NOESY data sets in H_2O and the dC(H5)−dC(H6) fixed distance of 2.45 Å for NOESY data sets in D_2O solution. A quadratic polynomial was fitted to the data points, and the initial slope was calculated from the linear fit of the quadratic curves to the first non-zero mixing time. The upper and lower bound ranges on the estimated interproton distances for nonexchangeable protons were determined based on the resolution of the cross-peaks in the two-dimensional contour plots and the quality of the NOE build-up plots.

The base proton to sugar H1′ proton NOE cross-peak in the shortest mixing time NOESY data set in D_2O were evaluated to qualitatively differentiate between *syn* (strong NOE) and *anti* (weak NOE) glycosidic torsion angles (Patel et al., 1982). The proton−proton vicinal coupling constants among sugar protons were analyzed from phase-sensitive COSY spectra to qualitatively distinguish between the C3′-*endo* and C2′-*endo* family of sugar puckers. The relative intensity of the NOE cross-peaks between base protons and their own and 5′-flanking sugar H2′, H2″, and H3′ protons were also used to qualitatively distinguish between the A-DNA and B-DNA families of helices for the modified duplex (van der Ven & Hilbers, 1988).

Molecular Mechanics Computations. Minimized potential energy calculations were carried out with DUPLEX, a molecular mechanics program for nucleic acids that performs potential energy minimizations in the reduced variable domain of torsion angle space (Hingerty et al., 1989). The

advantage of torsion space, compared to Cartesian space minimizations, is the vast diminution in the number of variables that must be simultaneously optimized, thereby permitting larger movements from a given starting conformation during minimization, as well as assurance of correct internal geometry and chirality.

DUPLEX uses a potential set similar to the one developed by Olson and co-workers for nucleic acids (Taylor & Olson, 1983) for which details have been published previously (Hingerty et al., 1989). Geometry and force field parameters, including partial charges, for the [AF]dG adduct were the same as those employed previously (Hingerty & Broyde, 1982; Broyde & Hingerty, 1983). A hydrogen-bond penalty function (Hingerty et al., 1989) was employed in all first-stage minimizations to aid the minimizer in locating the Watson−Crick hydrogen-bonded structures indicated by the NMR data. To locate minimum energy conformations with interproton distances available from the experimental NMR data, pseudopotentials (permitting upper and lower bound restraints) were added to the energy, as described previously (Norman et al., 1989; Schlick et al., 1990; Cosman et al., 1993). Briefly, the following functions were used:

$$F_N = W_N \sum_1^n (d - d_N)^2 \quad (1)$$

$$F_{NN} = W_{NN} \sum_1^n (d - d_{NN})^2 \quad (2)$$

The W's are adjustable weights (in the range 10−30 kcal/mol·Å^2). Weights in this range serve to guide the minimizer toward the structure defined by the NMR data while permitting the force field, whose predictive capabilities have been demonstrated (Hingerty et al., 1989; Singh et al., 1991), to play its part. d is the current value of the interproton distance, d_N is a target upper bound, and d_{NN} is a target lower bound. Equation 1 is implemented when d is greater than d_N, and eq 2 is implemented when d is less than d_{NN}. The functions are summed over all n target distances. All penalty functions were released in the last minimization steps to yield unrestrained final structures that are minimum energy conformations. F_N and F_{NN} can also be employed as relative indices of goodness-of-fit to the NMR data. Here the d values are the achieved distances in a given model and the W's are the weights employed in the search. F_N and F_{NN} are composites, reflecting the overall fit of all the achieved distances to their targets. They both adopt values of zero when all model distances are within the upper and lower NMR distance bounds. Small deviations from the NMR targets, with the uncertainty of the data, are accepted in computed models, and these therefore have non-zero F_N and F_{NN} values. Computations were carried out at the Department of Energy's National Energy Research Supercomputer Center and the National Science Foundation's San Diego Supercomputer Center.

RESULTS

Thermodynamic Stability of [AF]dG Opposite a Two-Base Deletion. The thermal transition midpoints (T_m) for the control dG·2del 12-mer duplex and the [AF]dG·2del 12-mer duplex **2** were measured at optical concentrations (10 μM in strands). The introduction of the covalently linked aminofluorene moiety into the dG·2del 12-mer duplex resulted in a remarkable 11 °C increase in T_m, from 22 °C for the control duplex to 33 °C for the adducted 12-mer duplex. Thermodynamic stabilization of carcinogen-adducted duplexes containing deletion sites has been previously observed for an [AF]dG adduct opposite a −1 deletion site (Mao et al., 1995), and [AAF]dG adduct opposite a −1 deletion site (Garcia et al., 1993) and *anti*-BPDE-dG adducts opposite a −1 deletion site (Ya et al., 1994). The observed stabilization on adduct formation permitted us to undertake NMR studies (at 3 mM concentrations) on the [AF]dG·2del 12-mer duplex at ambient temperature.

C1 − C2 − A3 − T4 − C5 − G6* − A7 − C8 − T9 − A10 − C11 − C12

G22-G21-T20-A19-G18 ——— G17-A16-T14-G15-G13

2

Exchangeable Nucleic Acid Protons. The exchangeable proton NMR spectrum (11.0−14.5 ppm) of the [AF]dG·2del 12-mer duplex in H_2O buffer, pH 7.0, at 1 °C is plotted in Figure 1A. Two well-resolved upfield-shifted imino protons at 11.53 and 12.12 ppm are detected in addition to several partially resolved exchangeable imino protons resonating between 12.8 and 14.0 ppm.

The expanded regions of the NOESY contour plot (150 ms mixing time) of the [AF]dG·2del 12-mer duplex in H_2O buffer, pH 7.0, at 1 °C are plotted in Figure 2. The imino and amino protons in the duplex have been assigned by standard procedures [reviewed in Patel et al. (1987) and van de Ven and Hilbers (1988)]. We detect imino to imino NOE connectivities between adjacent base pairs along the length of the modified duplex except between the imino protons of dG17, [AF]dG6, and dG18 residues centered about the lesion site. These NOE cross-peaks are traced in the expanded NOESY contour plot of the symmetrical 11.2−14.2 ppm region in Figure 2C with no NOE detected between the imino protons of dG17 (12.12 ppm) and dG18 (13.17 ppm) (boxed region, Figure 2C). The observed NOE patterns establish Watson−Crick pairing at all dG·dC pairs (deoxyguanosine imino to deoxycytidine amino NOE cross-peaks, Figure 2B) and all dA·dT base pairs (thymidine imino to deoxyadenosine H2 NOE cross-peaks, Figure 2B) in the [AF]dG·2del 12-mer duplex. The deoxyguanosine imino proton at 11.53 ppm is assigned to [AF]dG6 positioned opposite the −2 deletion site in the adduct duplex. It exhibits an NOE to its own averaged amino protons at 6.45 ppm (peak C, Figure 2B) and also a strong NOE to the H_2O resonance. Its upfield shift and rapid exchange with H_2O suggest that this deoxyguanosine imino proton of [AF]dG6 positioned opposite the deletion site most likely loops out of the helix and is accessible to solvent in the [AF]dG·2del 12-mer duplex.

The exchangeable proton chemical shifts for the central d(C5-[AF]G6-A7-C8)·d(G17-G18) segment of the [AF]-dG·2del 12-mer duplex are listed in Table 1 and for the entire adduct duplex in Table S1 of the supporting information.

The observed NOE patterns establish the formation of intact Watson−Crick dC8·dG17 and dC5·dG18 base pairs on either side of the [AF]dG6 lesion positioned opposite the two-base deletion site. The observed upfield shift of the dG17 imino proton possibly reflects its stacking with the aminofluorene ring of [AF]dG6 in the duplex.

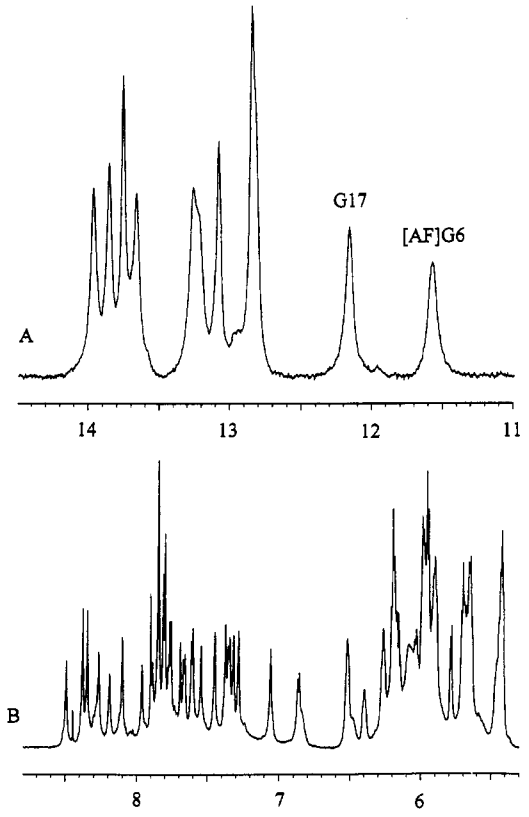

FIGURE 1: (A) Imino proton spectra (11.0−14.5 ppm) of the [AF]-dG·2del 12-mer duplex in H_2O buffer at 1 °C and (B) non-exchangeable proton spectra (5.3−8.8 ppm) of the [AF]dG·2del 12-mer duplex in D_2O buffer at 25 °C. The buffer was 0.1 M NaCl, 10 mM phosphate, 0.1 mM EDTA, at pH 7.0. The imino proton assignments of the [AF]dG6 and dG17 are shown over the resonances in the spectrum in A.

Nonexchangeable Nucleic Acid Protons. The non-exchangeable proton spectrum (5.3−8.8 ppm) of the [AF]dG·2del 12-mer duplex in D_2O, pH 7.0, at 25 °C is plotted in Figure 1B. The reasonably well resolved nucleic acid base and sugar protons as well as aminofluorene protons were assigned based on an analysis of through-space distance connectivities in NOESY data sets as a function of mixing time and through-bond connectivities in COSY and TOCSY data sets recorded in D_2O buffer, pH 7.0, at 25 °C.

The sequential NOE connectivities between the base protons (6.7−8.6 ppm) and the sugar H1′ and deoxycytidine H5 protons (5.3−6.7 ppm) of the [AF]dG·2del 12-mer duplex in D_2O buffer, pH 7.0, at 25 °C are shown in Figure 3. The NOE connectivities from the base proton (purine H8 or pyrimidine H6) to its own and 5′-flanking sugar H1′ protons have been traced along the duplex from dC1 to dC12 on the modified strand and from dG13 to dG22 on the complementary strand. This tracing is shown for the central segment extending from dA3 to dT9 on the modified strand (solid line, Figure 3) and from dA16 to dA19 on the unmodified complementary strand (dashed line, Figure 3). The sequential NOEs for the modified strand were uninterrupted except at the dC5-[AF]dG6 step, where the purine H8 proton is absent following AF modification at the C^8 position of dG6 in the adduct duplex. The cross-peak between dG17(H1′) and dG18(H8) were weak (see arrow labeled a, Figure 3) for the tracing of sequential NOEs in the complementary strand, indicating a greater-than-normal distance between these two protons. These base and sugar

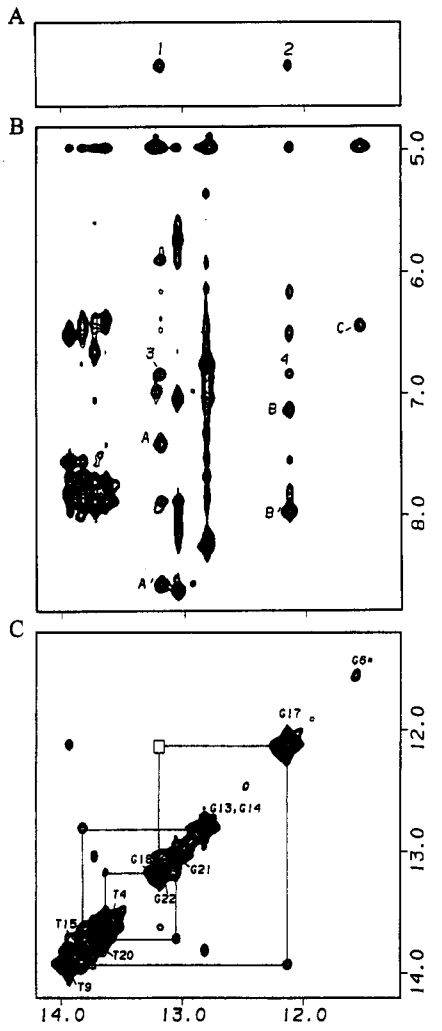

FIGURE 2: Expanded NOESY (150 ms mixing time) contour plots of the [AF]dG·2del 12-mer duplex in H_2O buffer at 1 °C. (A) NOE connectivities between the imino protons (11.2−14.2 ppm) and the AF methylene protons (2.5−3.5 ppm). The carcinogen−DNA cross-peaks 1 and 2 are assigned as follows: 1, G18(NH1)-AF(H9a,b); 2, G17(NH1)-AF(H9a,b). (B) NOE connectivities between the imino protons (11.2−14.2 ppm) and the base and amino protons regions (4.8−8.8 ppm). The NOE cross-peaks involving the imino protons are labeled in the figure as follows: A′ and A, G18(NH1)-C5(NH_2-4b,e); B′ and B, G17(NH1)-C8(NH_2-4b,e); C, [AF]G6(NH1)-[AF]G6(NH_2-2). The carcinogen−DNA NOE cross-peaks 3 and 4 are assigned as follows: 3, G18(NH1)-AF(H4); 4, G17(NH1)-AF(H4). (C) NOE connectivities in the symmetrical (11.2−14.2 ppm) region. The imino assignments are labeled along the diagonal. The lines trace the NOE connectivities between adjacent base pairs starting at dG22 toward one end of the helix and proceeding to dG13 toward the other end of the helix. The connectivity between the imino protons of dG17 and that of dG18 is missing and marked by a box.

H1′ proton assignments have been confirmed by cross checks in other regions of the NOESY contour plot (Figure 4A), as well as from COSY (Figure 4B) and TOCSY plots to yield a complete set of base and sugar H1′, H2′, H2″, H3′, and H4′, proton assignments for the [AF]dG·2del 12-mer duplex.

The nonexchangeable proton chemical shifts for the central d(C5-[AF]G6-A7-C8)·d(G17-G18) segment in the [AF]-dG·2del 12-mer duplex are listed in Table 1 and for the entire adduct duplex are listed in Table S2. Proton chemical shift differences for the central segment between the adduct duplex and the modified control duplex are given in Table S3 of the supporting information.

Table 1: Proton and Phosphorus Chemical Shifts of the d(C5-[AF]G6-A7-C8)·d(G17-G18) Segment of the [AF]dG·del 12-mer Duplex in Aqueous Buffer

	exchangeable proton chemical shifts, ppm, 1 °C		
	G(NH1)	G(NH_2-2)	C(NH_2-4)
dC5·dG18	13.17		7.40,[a] 8.58[b]
[AF]dG6	11.53	6.45	
dC8·dG17	12.12		7.15,[a] 7.97[b]

	nonexchangeable proton and phosphorus chemical shifts, ppm, 25 °C						
	H8/H6	H2/H5	H1′	H2′, H2″	H3′	H4′	$^{31}P^c$
dC5	6.83	5.89	5.90	1.07, 1.94	4.62	4.01	−3.36
[AF]dG6			5.68	3.11, 2.25	4.82	4.47	−4.39
dA7	8.38	7.96	6.51	2.99, 2.71	5.12	4.47	−4.06
dC8	7.85	6.08	6.06	2.13, 2.52	4.88	4.28	−4.16
dG17	7.37		5.42	2.12, 2.07	5.08	4.17	−3.60
dG18	8.19		5.68	2.81, 2.89	5.03	4.33	−4.23

[a] Exposed amino proton. [b] Hydrogen-bonded amino proton. [c] ^{31}P chemical shift corresponds to residue n for the (n)-^{31}P-$(n+1)$ step.

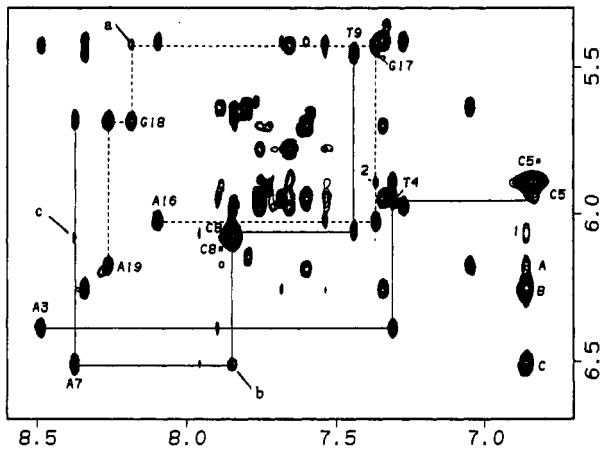

FIGURE 3: An expanded NOESY (300 ms mixing time) contour plot of the [AF]dG·2del 12-mer duplex in D_2O buffer at 25 °C establishing distance connectivities between the base (purine H8 and pyrimidine H6) protons (6.7−8.6 ppm) and the sugar H1′ and deoxycytidine H5 protons (5.3−6.7 ppm). The NOE connectivities between the base and their own and the 5′-flanking sugar H1′ protons from dA3 to dT9 on the modified strand are shown by solid lines and from dA16 to dA19 on the unmodified partner strand are shown by dashed lines. The assignments label the base to their own sugar H1′ NOEs, while the deoxycytidine H6−H5 NOEs are designated by asterisks. Note the unusual upfield shift of the H6 proton of dC5 to 6.83 ppm. Note that the NOE cross-peak at the dC5-[AF]dG6 is missing because of the absence of an H8 proton for [AF]dG6. The carcinogen−carcinogen NOE cross-peaks A−C between aminofluorene protons are assigned as follows: A, AF(H4)-AF(H6); B, AF(H4)-AF(H3); C, AF(H4)-AF(H5). The carcinogen−DNA NOE cross-peaks are assigned as follows: 1, AF(H4)-C8(H5); 2, AF(H8)-G17(H8). The weak NOE cross-peaks labeled a−c are assigned as follows: a, G18(H8)-G17(H1′); b, C8(H6)-A7(H1′); c, A7(H8)-C8(H5).

It should be noted that relative to the control duplex, large upfield chemical shifts are observed on adduct formation at the H6 (−0.49 ppm) base and the H2′ (−0.71 ppm) sugar protons of the dC5 residue (Table S2, Figures 3 and 4) located 5′ to the lesion site on the modified strand. By contrast, downfield shifts are observed on adduct formation at the H2′ (+0.94 ppm) and H1′ (+0.29 ppm) sugar protons of the [AF]dG6 residue (Table S2). Further, we observe an inversion in the characteristic H2′ and H2″ sugar cross-peak patterns at the lesion site with the H2′ proton chemical shift

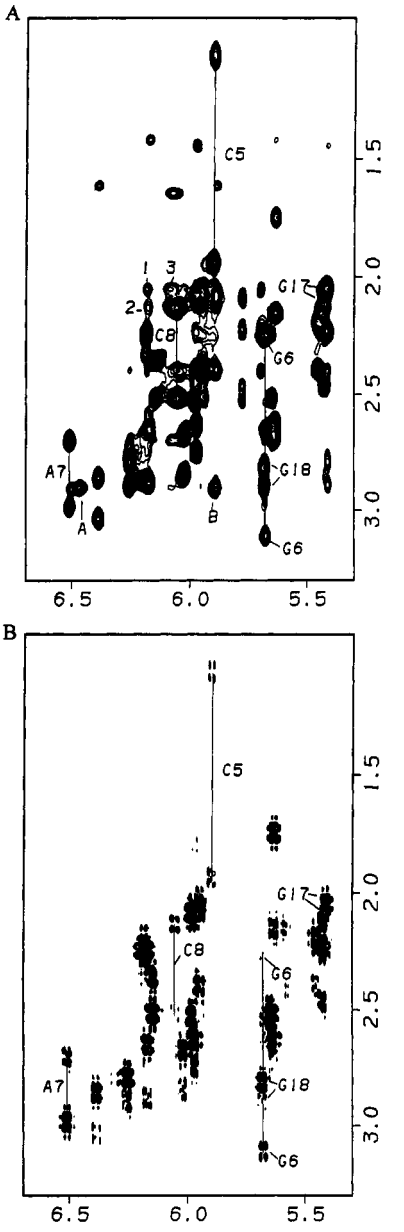

FIGURE 4: (A) An expanded NOESY (300 ms mixing time) contour plot of the [AF]dG·2del 12-mer duplex in D_2O buffer at 25 °C showing NOE between the sugar H1′ protons (5.3−6.7 ppm) and H2′ and H2″ protons (0.9−3.3 ppm). The NOE cross-peaks A and B between aminofluorene protons are assigned as follows: A, AF(H1)-AF(H9a,b), and B, AF(H8)-AF(H9a,b). The carcinogen−DNA NOE cross-peaks 1−3 are assigned as follows: 1, G17(H2″)-AF(H6); 2, G17(H2′)-AF(H6); 3, G17(H2″)-AF(H7). (B) An expanded phase sensitive COSY contour plot of the [AF]dG·2del 12-mer duplex in D_2O buffer at 25 °C establishing coupling connectivities between the H1′ protons (5.3−6.7 ppm) and H2′ and H2″ protons (0.9 to 3.3 ppm). In both A and B the H2′ and H2″ protons of dC5, [AF]dG6, dA7, dC8, dG17, and dG18 are connected by lines and labeled. The H2′ protons resonate upfield of the H2″ protons for the majority of these residues except for [AF]dG6, dA7, and dG17, for which the H2″ protons resonate upfield of the H2′ proton.

(3.11 ppm) of [AF]dG6 shifting dramatically downfield in the adduct duplex (Figure 4). In addition, downfield chemical shifts are observed on adduct formation at the H8 (+0.32 ppm) and H1′ (+0.59 ppm) base protons of the unpaired dA7 residue.

Aminofluorene Protons. The nonexchangeable aminofluorene protons were assigned from an analysis of through-

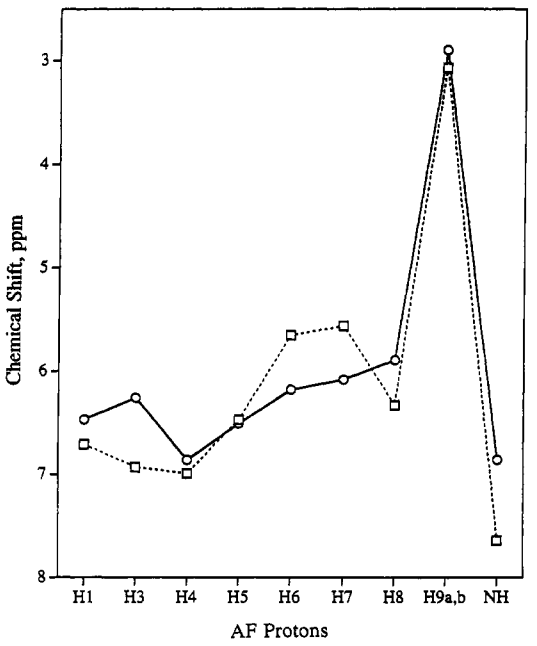

FIGURE 5: Plot comparing the aminofluorene ring proton chemical shifts in the [AF]dG·2del 12-mer duplex (circles) and the [AF]-dG·1del 11-mer duplex (squares). The chemical shift values for the aminofluorene protons in the [AF]dG·2del 12-mer duplex are as follows: AF(H1), 6.47 ppm; AF(H3), 6.26 ppm; AF(H4), 6.86 ppm; AF(H5), 6.51 ppm; AF(H6), 6.18 ppm; AF(H7), 6.08 ppm; AF(H8), 5.89 ppm; AF(H9a,b), 2.90 ppm; AF(NH), 6.86 ppm.

space and through-bond two dimensional spectra of the [AF]-dG·2del 12-mer duplex recorded in D_2O buffer, pH 7.0, at 25 °C. The H1 and H8 protons were assigned based on NOEs to the geminal H9a,b protons (2.90 ppm) within the aminofluorene ring. The H1, H3, and H4 protons along one edge of the aminofluorene ring can be differentiated from the H5−H8 protons on the opposite edge following analysis of coupling patterns observed in COSY and TOCSY spectra and from NOE cross-peaks observed in NOESY spectra. The exchangeable aminofluorene NH proton (6.86 ppm) was assigned on the basis of the strong NOE to the [AF]dG6(H1′) proton in the NOESY spectrum of the [AF]dG·2del 12-mer duplex in H_2O buffer. The nonexchangeable aminofluorene proton chemical shifts in the [AF]dG·2del 12-mer duplex are listed in the caption to Figure 5 and are plotted together with their counterparts in the [AF]dG·1del 11-mer duplex in Figure 5. The aminofluorene aromatic ring protons resonate between 5.5 and 7.0 ppm with both similarities and differences in individual proton chemical shifts for the duplexes containing [AF]dG opposite single (squares) and double (circles) deletion sites (Figure 5).

Carcinogen−DNA NOEs and Restraints. We observe a set of carcinogen−DNA NOEs centered about the lesion site in the [AF]dG·2del 12-mer duplex which have been categorized on the basis of whether they involve exchangeable or nonexchangeable protons. The corresponding carcinogen−DNA distance restraints deduced from NOE build-up curves for nonexchangeable protons and defined by lower and upper bounds in the [AF]dG·2del 12-mer duplex are listed in Table 2. We also included DNA−DNA distance restraints involving the unpaired dA7 residue within the d([AF]G6-A7-C8) segment in the computations (Table 3) in order to define the alignment of dA7 relative to the [AF]dG6 adduct and the −2 deletion site.

Table 2: Comparison of Input Carcinogen−DNA Distance Bounds for the d(C5-[AF]G6-A7-C8)·d(G17-G18) with Those Observed for the Unrestrained Solution Conformation of the [AF]dG·2del 12-mer Duplex

	carcinogen−DNA distances, Å	
	exptl bounds	obsd bounds
exchangeable protons		
[AF]G6(H1′)-AF(NH)	2.2−3.5	3.01
A7(H4′)-AF(NH)	3.0−5.0	3.92
G17(NH1)-AF(H9a,b)	3.0−5.0	2.62, 4.08
G17(NH1)-AF(H4)	3.0−5.5	5.09
G18(NH1)-AF(H4)	3.0−5.5	5.99
G18(NH1)-AF(H9a,b)	2.8−5.0	3.33, 4.85
nonexchangeable protons		
[AF]G6(H1′)-AF(H3)	3.0−5.0	2.23
A7(H2)-AF(H1)	>5.0	4.77
A7(H2)-AF(H9a,b)	>5.0	7.64, 7.58
A7(H4′)-AF(H3)	3.0−4.5	3.25
A7(H4′)-AF(H4)	4.0−5.5	4.89
G17(H8)-AF(H8)	3.5−5.5	5.15
G17(H2′)-AF(H6)	3.0−6.0	7.11
G17(H2″)-AF(H6)	2.5−5.5	5.74
G17(H2″)-AF(H7)	2.5−5.5	3.61

Table 3: Comparison of Input DNA−DNA Distance Bounds for the d([AF]G6-A7-C8) Segment with Those Observed for the Unrestrained Solution Conformation of the [AF]dG·2del 12-mer Duplex

	DNA−DNA distances, Å	
	exptl bounds	obsd bounds
[AF]G6(H1′)-A7(H8)	3.0−5.0	4.61
[AF]G6(H2′)-A7(H8)	2.8−4.0	3.48
[AF]G6(H2″)-A7(H8)	2.3−3.4	2.56
A7(H8)-A7(H2′)	2.0−2.8	2.23
A7(H8)-A7(H2″)	2.2−3.5	3.51
A7(H8)-A7(H1′)	2.5−4.0	3.75
A7(H8)-A7(H3′)	3.0−4.5	4.38
A7(H1′)-C8(H6)	3.0−5.0	3.13
A7(H1′)-C8(H5)	2.2−4.0	3.45
A7(H2′)-C8(H6)	>5.0	5.07
A7(H4′)-C8(H6)	2.5−3.8	2.61
A7(H4′)-C8(H5)	3.5−5.0	4.72

The observed NOEs between the aminofluorene H4 and H9a,b protons and the imino protons of dG17 and dG18 place the aminofluorene between the dC5·dG18 and dC8·dG17 base pairs in the adduct duplex. We observe NOEs between the aminofluorene H6 and H7 protons at the [AF]dG lesion site and the sugar H2′ and H2″ protons of dG17 as well as between the aminofluorene H8 proton and base H8 proton of dG17 in the adduct duplex. These NOEs establish that the aminofluorene ring edge furthest from the covalent linkage site is positioned near the base and sugar protons of dG17 on the partner strand of the [AF]dG·2del 12-mer duplex. The long axis of the aminofluorene ring must be approximately parallel to the long axis of the flanking base pairs if its H6−H8 protons are to interact with the partner strand across from the lesion site.

The observed large upfield chemical shift of the H6 proton (−0.49 ppm) located on the major groove edge of dC5 combined with upfield shifts for dC5 sugar H2′ and H2″ protons requires that the modified deoxyguanosine be displaced into the major groove and positioned over the major groove base edge and sugar ring of dC5 in the adduct duplex. This alignment can only be achieved if the [AF]dG6 adopts a *syn* glycosidic torsion angle in the adduct duplex.

Several NOEs characteristic of a regular B-DNA helix are either very weak or are not observed for the d(A7−C8) step in the [AF]dG·2del 12-mer duplex. These include the observation of a very weak NOE between the A7(H8) and C8(H5) protons (see arrow marked c, Figure 3) and the absence of an NOE between the A7(H2′) and C8(H6) protons. These results suggest that the dA7 residue is most likely looped out of the helix in the [AF]dG·2del 12-mer duplex. This conclusion is further supported by the observed NOEs between the imino proton of dG17 and the H4 (peak 4, Figure 2B) and H9a,b (peak 2, Figure 2A) aminofluorene protons. These distance connectivities can only be achieved if the dA7 is looped out of the helix to allow the aminofluorene ring to stack with the dC8·dG17 base pair. The weak intensity of the NOE cross-peak between H8 and H1′ protons of dA7 in the 50 ms mixing time NOESY experiment establishes that the glycosidic torsion angle of dA7 is in the *anti* conformation.

Carbon Spectra. The expanded contour plot of a natural abundance proton−carbon HMQC correlation experiment that correlates the H1′ and C1′ chemical shifts of individual residues for the [AF]dG·2del 12-mer duplex in D_2O buffer, pH 7.0, at 25 °C is plotted in Figure 6A. The carbon resonances are assigned on the basis of the known H1′ proton assignments in the adduct duplex. The C1′ chemical shift assignments for each individual residue in the d(T4-C5-[AF]G6-A7-C8-T9)·d(A16-G17-G18-A19) segment are labeled in Figure 6A. We note that the C1′ chemical shift of [AF]dG6 (86.96 ppm) is ~3 ppm downfield of its neighboring dG17 (83.26 ppm) and dG18 (84.41 ppm) residues in the adduct duplex (Figure 6A). It has been previously established that downfield sugar C1′ carbon chemical shifts ranging up to 5 ppm are observed for DNA residues adopting *syn* glycosidic torsion angles provided that they retain C2′-*endo* sugar pucker geometries (Ghose et al., 1994; Greene et al., 1995). We detect a strong coupling cross-peak between the H1′ (5.68 ppm) and H2′ (3.11 ppm) protons of [AF]dG6 (Figure 4B) placing this sugar in the C2′-*endo* range. The ~3 ppm downfield sugar C1′ carbon chemical shift of [AF]dG6 identifies a *syn* glycosidic torsion angle at this modified residue in the [AF]dG·2del 12-mer duplex.

Phosphorus Spectra. The proton-decoupled phosphorus spectrum of the [AF]dG·2del 12-mer duplex has been recorded in D_2O buffer, pH 7.0, at 25 °C. The phosphorus resonances are dispersed over a 1 ppm range with several resonances shifted to low field of the −4.0 to −4.5 ppm spectral region characteristic of an unperturbed B-DNA phosphodiester backbone. The phosphorus resonances have been assigned from an analysis of the proton-detected phosphorus−proton heteronuclear correlation experiment, and the expanded contour plot is shown in Figure 6B. Each phosphorus resonance can be correlated to the 5′-linked H3′ proton and the 3′-linked H4′, H5′, and H5″ protons. The phosphorus resonances are assigned on the basis of the known H3′ and H4′ proton assignments in the adduct duplex. The phosphorus assignments for the individual steps in the d(T4-C5-[AF]G6-A7-C8-T9)·d(A16-G17-G18-A19) segment of the adduct duplex are labeled in Figure 6B and listed in Table 1. The phosphorous chemical shifts for the dC5-[AF]dG6 (−3.36 ppm) and dG17-dG18 (−3.60 ppm) steps are shifted to low field of the −4.0 to −4.5 ppm unperturbed phosphodiester backbone chemical shift range.

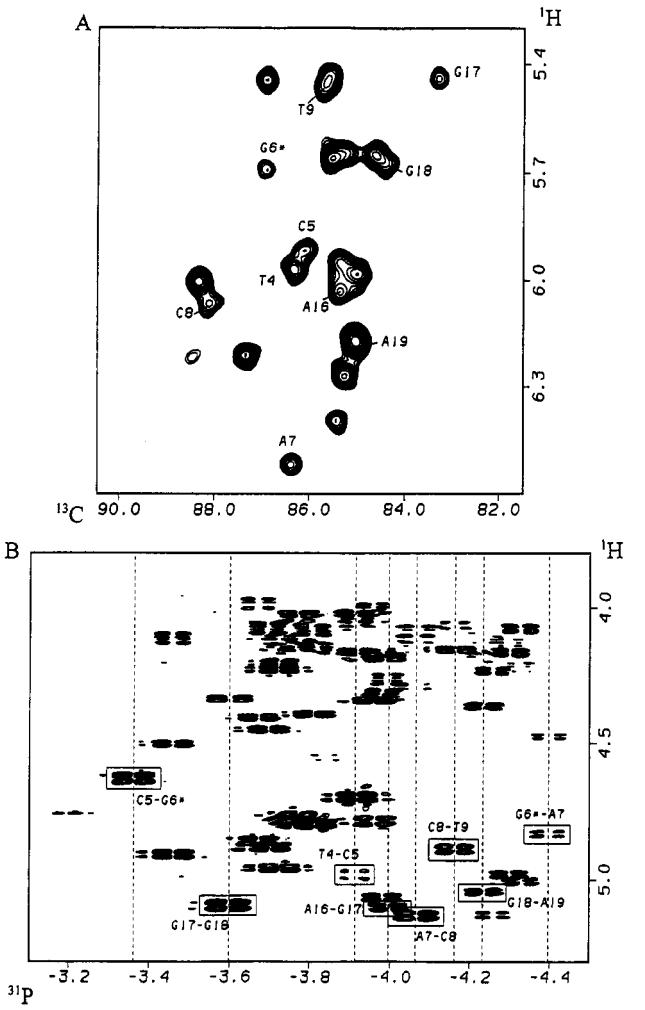

FIGURE 6: (A) An expanded contour plot of ^{1}H−^{13}C heteronuclear multiple-quantum coherence (HMQC) experiment on the [AF]-dG·2del 12-mer duplex in D_2O buffer at 25 °C. The C1′ assignments are marked for residues in the d(T4-C5-[AF]G6-A7-C8-T9)·d(A16-G17-G18-A19) segment. (B) An expanded contour plot of the proton-detected phosphorus−proton heteronuclear correlation experiment on the [AF]dG·2del 12-mer duplex in D_2O buffer at 25 °C. The phosphorus assignments are listed for steps centered about the lesion site. The correlation cross-peaks between the phosphorus and its 5′-flanking sugar H3′ protons are boxed.

Molecular Mechanics Computations. The search strategy employed begun with a B-DNA (Arnott et al., 1976) central d(T4-C5-[AF]G6-A7-C8-T9)·d(A16-G17-G18-A19) 6/4 base pair segment of the [AF]dG·2del 12-mer duplex. The computations were guided by the carcinogen−DNA and DNA−DNA restraints listed in Tables 2 and 3, respectively. The AF−DNA orientation space was searched with 16 energy minimization trials in which the linkage torsion angles α' ([AF]dG6(N^9)−[AF]dG6(C^8)−[AF](N)−[AF](C^2)) and β' ([AF]dG6(C^8)−[AF](N)−[AF](C^2)−[AF](C^1)) were each started at 0, 90, 180, and 270° in all combinations, and the DNA starting conformation was the B-form except for a *syn* (χ = 60°) glycosidic torsion for the [AF]dG6 residue as required by the experimental ^{13}C chemical shift data. Searching orientation space at 90° intervals of α' and β' is a robust procedure for locating all the important potential energy wells because our minimization protocol permits torsion angle variations of up to 100° in each minimization step (Hingerty et al., 1989). Consequently, energy minima in each quadrant of α' and β' are accessible and the reduced

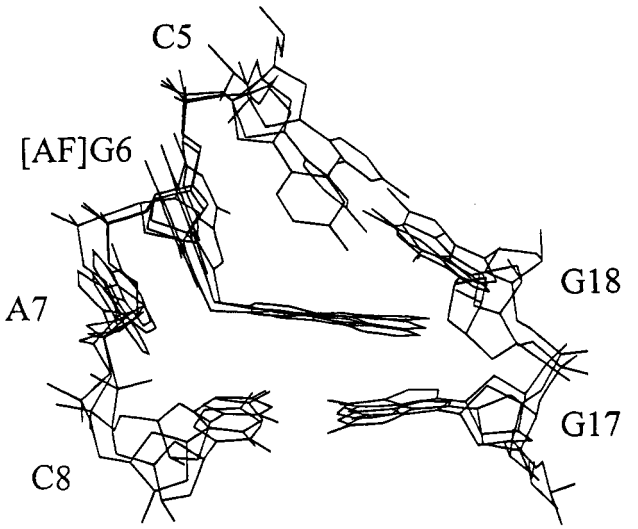

FIGURE 7: The superposition of the three d(C5-[AF]G6-A7-C8)·d(G17-G18) segments of the computed conformations that best fit the NMR data of the [AF]dG·2del 12-mer duplex. These were obtained from the 16 trials which searched conformational space using the program DUPLEX and were guided by the NMR-based carcinogen–DNA restraints (Table 2). View looking into the major groove and normal to the helix axis of the central segments.

variable domain of torsion angle space greatly enhances the likelihood of finding the important structures. In these trials, the DUPLEX hydrogen-bond penalty function (Hingerty et al., 1989) for Watson–Crick base pairing was utilized at the dT4·dA19, dC5·dG18, dC8·dG17, and dT9·dA16 base pairs, since the NMR data indicated that these hydrogen bonds were present.

Of the 16 computed conformations of the d(T4-C5-[AF]-G6-A7-C8-T9)·d(A16-G17-G18-A19) segment, one conformation had the lowest energy and very low goodness-of-fit indices. This conformation had energy of −176.3 kcal/mol and goodness-of-fit values for eqs 1 and 2 of 2.5 and 3.0, respectively, with $W = 15$ kcal/mol·Å^2. The second- and third-ranked conformations had energies of −158.5 and −158.2 kcal/mol and goodness-of-fit indices for eq 1 of 5.2 and 4.0, respectively, and for eq 2 of 4.3 and 1.0, respectively. A superpositioned view of the d(C5-[AF]G6-A7-C8)·d(G17-G18) segment of these three conformations is plotted in Figure 7. The d(C5-[AF]G6-A7-C8-T9)·d(A16-G17-G18) segment of the lowest energy conformation was employed in building the [AF]dG·2del 12-mer duplex. For this purpose, an unmodified energy-minimized B-form dG6·2del 12-mer duplex was first computed. The d(C5-[AF]G6-A7-C8-T9)·d(A16-G17-G18) segment was then embedded in the dG6·2del 12-mer duplex by replacement of residues dC5, dG6, dA7, dC8, and dT9 and their partners dA16, dG17, and dG18, followed by energy minimization with restraints. Subsequently, the hydrogen-bond penalty function and the distance restraints were released with energy minimization in one step, yielding a final unrestrained minimum energy conformation of the [AF]dG6·2del 12-mer duplex in which the C^9-containing edge of aminofluorene faces the major groove.

Solution Conformation of the [AF]dG Adduct Duplex. A view normal to the helix axis and looking into the major groove of the central d(T4-C5-[AF]G6-A7-C8-T9)·d(A16-G17-G18-A19) segment of the NMR energy-minimized conformation of the [AF]dG·2del 12-mer duplex is shown

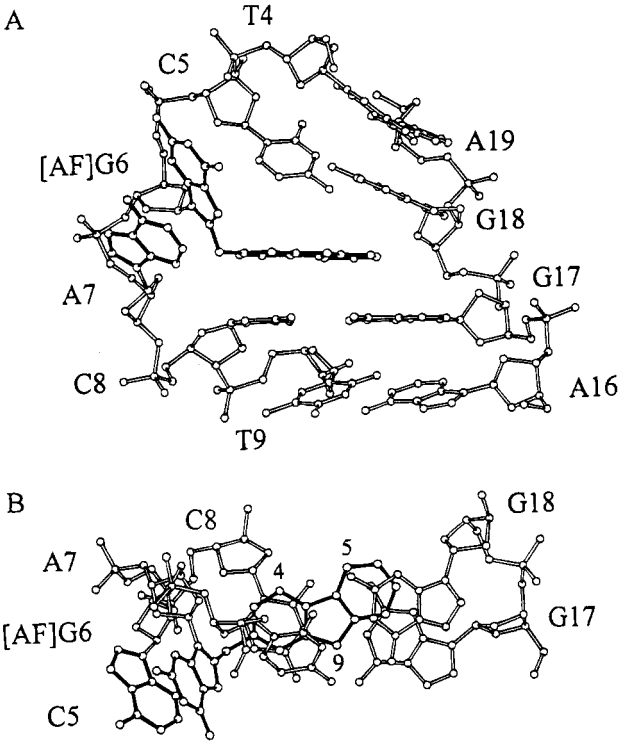

FIGURE 8: (A) View looking into the major groove and normal to the helix axis of the central d(T4-C5-[AF]G6-A7-C8-T9)·d(A16-G17-G18-A19) segment of the [AF]dG·2del 12-mer duplex solution conformation. The AF ring system is shown in darkened bonds and is intercalated between the dC5·dG18 and dC8·dG17 base pairs. The modified dG6 base is displaced into the major groove and is directed toward its 5′-neighbor dC5 in the sequence. The unpaired dA7 is also displaced into the major groove and is partially stacked with the modified dG6. (B) View looking down the helix axis for the d(C5-[AF]G6-A7-C8)·d(G17-G18) segment in the solution conformation of the [AF]dG·2del 12-mer duplex. Figures were prepared using Molscript VI.1 (Kraulis, 1991).

in Figure 8A. The corresponding conformation for the entire adduct duplex is shown in Figure S1 in the supporting information. The covalently linked aminofluorene ring intercalates between flanking Watson–Crick dC5·dG18 and dC8·dG17 base pairs by displacing the deoxyguanosine ring of [AF]dG6 and the deoxyadenosine ring of dA7 into the major groove (Figure 8A). The major groove face of the sugar ring of dC5 is positioned over the deoxyguanosine base plane of [AF]dG6 which is directed toward the 5′-end of the modified strand and tilted relative to the helix axis (Figure 8A). The adenine ring of dA7 is also directed toward the 5′-end and stacked with the guanine ring of [AF]dG6. The aminofluorene is intercalated between the dC5·dG18 and dC8·dG17 base pairs, and greater stacking is observed with the dC8·dG17 base pair. The dC5·dG18 pair is propeller-twisted by −34.2° and buckled by 26.5° (Figure 8A) [computed using the approach of Babcock et al. (1993)].

A view looking down the helix axis of the central d(C5-[AF]G6-A7-C8)·d(G17-G18) segment of the NMR energy-minimized conformation of the [AF]dG·2del 12-mer duplex is shown in Figure 8B. The view emphasizes the overlap geometry between the aminofluorene ring system and the flanking dC5·dG18 and dC8·dG17 base pairs. The long axis of the aminofluorene ring of AF is approximately parallel to the long axis of the dC5·dG18 and dC8·dG17 base pairs (Figure 8B). In addition, the looped out purine bases of [AF]dG6 and dA7 stack on each other in the solution

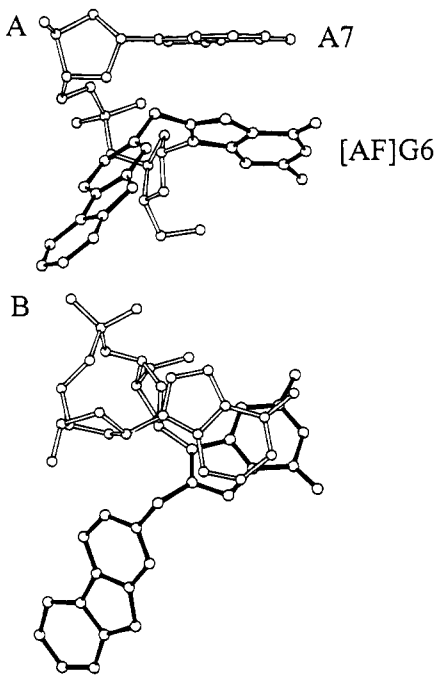

FIGURE 9: Two views emphasizing the relative alignments of the purine rings of [AF]dG6 and dA7 in the [AF]dG6-dA7 segment of the [AF]dG•2del 12-mer duplex conformation. Views looking (A) into the plane and (B) normal to the plane of the dA7 purine ring.

conformation of the [AF]dG•2del 12-mer duplex (Figure 9).

The carcinogen−base linkage site for the [AF]dG6 residues is defined by the torsion angles α' ([AF]dG6(N^9)−[AF]-dG6(C^8)−[AF](N)−[AF](C^2) = 87° and β' ([AF]dG6(C^8)−[AF](N)−[AF](C^2)−[AF](C^1) = 80°. The β' = 80° orientation directs the C^9-containing edge of aminofluorene toward the major groove (Figure 8B) for the [AF]dG•2del 12-mer duplex. The glycosidic torsion angles, sugar puckers, and backbone torsion angles for the d(T4-C5-[AF]G6-A7-C8-T9)•d(A16-G17-G18-A19) segment of the [AF]dG•2del 12-mer duplex are listed in Table S4. The following torsion angles deviate from standard B-DNA values. The χ(O4′−C1′−N1−C2) glycosidic torsion of the dC5 residue is high *anti* (χ = 315°) rather than *anti*, and the χ of the [AF]dG6 residue is *syn* (59°). The ξ(O3′−P) torsion angle of the dA7 residue (ξ = 105°) is between *gauche*$^+$ (60°) and *trans* (180°) rather than in the normal *gauche*$^-$ domain (300°). The torsion angle β(C5′−O5′) of the dC8 residue adopts a value of 121°, and β of dG18 is 246°, while standard B-DNA values are more closely centered at 180°. The pseudorotation parameter of the dC8 is 78°, corresponding to the O4′-*endo* domain in the [AF]dG•2del 12-mer duplex. Other torsion angles and pseudorotation parameters are within or near ranges observed in B-DNA crystals (Table S4).

DISCUSSION

Spectral Quality and Thermal Stability. The proton NMR spectra of the [AF]dG•2del 12-mer duplex in H_2O buffer at 1 °C (Figure 1A) and in D_2O buffer at 25 °C (Figure 1B) are well enough resolved to permit assignment of the proton resonances of both DNA and aminofluorene in the adduct duplex. This in turn has permitted the identification of NOEs around the −2 deletion site and provided sufficient restraints (Tables 2 and 3) to define the solution conformation at the [AF]dG•2del 12-mer duplex. The observed stabilization of the [AF]dG•2del 12-mer duplex relative to its control dG•2del 12-mer duplex aided the structural characterization by permitting collection of the experimental NMR data at ambient temperature.

Conformation of the Modified Deoxyguanosine. The glycosidic torsion angle of [AF]dG6 is in a *syn* conformation in the [AF]dG•2del 12-mer duplex. This observation is in accord with our earlier study on the [AF]dG opposite a −1 deletion site (Mao et al., 1995). The standard approach for distinguishing *syn* from *anti* deoxyguanosine glycosidic torsion angles is based on the magnitude of the NOE between the deoxyguanosine H8 proton and its own H1′ proton (Patel et al., 1982). This approach cannot be used for [AF]dG6 since the H8 proton is replaced by the AF ring. The [AF]-dG6 glycosidic torsion angle was initiated in the *syn* range in the computations based on the chemical shift patterns of the [AF]dG6 residue in the adduct duplex. The C1′ carbon of the modified deoxyguanosine was shifted downfield (~3 ppm) from the corresponding chemical shift of the adjacent dG17 and dG18 deoxyguanosine residues (Figure 6A). The downfield shift at the C1′ of [AF]dG6 due to a *syn* alignment is probably larger than 3 ppm since one expects upfield ring current contributions due to the mutual stacking of [AF]dG6 and dA7 in the structure of the [AF]dG•2del 12-mer duplex (Figures 8 and 9). A deoxyguanosine C1′ downfield shift of this magnitude has been identified with a *syn* glycosidic torsion angle for residues with C2′-*endo* sugar puckers (Greene et al., 1995). In addition we observe an unusual downfield shift for the H2′ proton (3.11 ppm) of the [AF]-dG6 residue in the [AF]dG•2del 12-mer duplex (Figure 4). Similar downfield shifts have been observed in previous NMR studies in which the [AF]dG is positioned opposite a −1 deletion site (Mao et al., 1995), a dA base substitution site (Norman et al., 1989), or dG and dI base substitution sites (Abuaf et al., 1995). In all these cases, a *syn* glycosidic torsion angle was established for the [AF]dG6 residue at the adduct site.

The intercalation of the AF ring results in the displacement of the modified deoxyguanosine ring into the major groove. The displaced modified deoxyguanosine is oriented in such a way that its long axis is inclined relative to the helix axis and pointed toward the 5′-side. One face of the modified deoxyguanosine ring stacks with the major groove base (H6) and sugar (H2′, H3′) protons of dC5 while the other face stacks with the looped out deoxyadenosine ring of the dA7 residue. This stacking alignment readily explains the upfield proton shifts of the major groove facing protons of the dC5 residue in the spectrum of the [AF]dG•2del 12-mer duplex (Table S3).

The imino proton of [AF]dG6 (11.53 ppm) falls in a range characteristic of non-hydrogen-bonded imino protons. This result is consistent with the exposed alignment of the imino proton of [AF]dG6 in the conformation of the [AF]dG•2del 12-mer duplex (Figure 8A). Similarly, the chemical shift of the amino protons (6.45 ppm) of [AF]dG6 is consistent with both amino protons being exposed to solvent rather than being hydrogen-bonded to acceptor groups.

Conformation of the Unpaired dA7. The dA7 glycosidic torsion angle was initiated in the *anti* range in the computations based on the NOE cross-peak patterns in the 50 ms NOESY data set of the [AF]dG•2del 12-mer duplex. The looped out dA7 is positioned in the major groove and stacks with the purine ring of the [AF]dG6 residue in the solution conformation of the adduct duplex (Figure 8A). This

alignment is supported by both NOE and chemical shift patterns. The displacement of the dA7 residue from the helix results in a break in the sequential connectivities at the dA7-dC8 step. Thus, the H6 proton of dC8 does not exhibit NOEs to the H8 and H2′ protons of dA7 and a weak NOE to the H1′ proton of dA7 (peak b, Figure 3) in the adduct duplex. The sugar protons (H1′, H2′, H2″, H3′, and H4′) of the dA7 in the [AF]dG·2del 12-mer duplex are downfield relative to their counterparts in the control dG·2del 12-mer duplex (Table S3) consistent with displacement of the dA7 out of the helix.

By contrast, regular sequential NOE connectivities are observed at the [AF]dG6-dA7 step, suggesting that these bases, which are both looped out of the helix, stack on each other. Indeed, the H8 and H2 protons of dA7 exhibit chemical shifts characteristic of a stacked residue. In addition, the sugar (H1′, H2′, 2″, H3′, and H4′) protons of [AF]dG6 in the [AF]dG·2del 12-mer are upfield of their counterparts in the [AF]dG·1del 11-mer duplex. This must reflect the stacking of [AF]dG6 and dA7 in the former case of a −2 deletion site (Figure 9) and the lack of the stacking due to the absence of an adjacent unpaired deoxyadenosine in the latter case of a −1 deletion site.

Intercalation of the Aminofluorene Ring into the Helix. A set of carcinogen−DNA NOEs between AF ring protons and the base and sugar protons on the flanking dC5·dG18 and dC8·dG17 base pairs define the intercalation of the AF ring into the DNA helix in the [AF]dG·2del 12-mer duplex (Table 2). The observed NOE restraints between the intercalated AF ring (H4, H9a, and H9b) protons and the imino protons of dG17 and dG18 which flank the intercalation site are satisfied in the solution conformation of the adduct duplex (Table 2). The aromatic AF protons resonate between 5.80 and 6.90 ppm in the [AF]dG·2del 12-mer duplex (this study) and between 5.55 and 7.00 ppm in the [AF]dG·1del 11-mer duplex (Mao et al., 1995) (Figure 5). These upfield chemical shifts are consistent with intercalation of the AF ring between base pairs for the [AF]dG adduct duplex opposite −2 and −1 deletion sites. By contrast, the AF protons resonate in the 7.6−8.0 ppm range for one of two interconverting conformations when the [AF]dG adduct is positioned opposite dC, consistent with alignment of the AF ring in the groove of the duplex for that conformation (Eckel & Krugh, 1995).

The relative placement of the various edges of the AF ring relative to the flanking base pairs is defined by the carcinogen−DNA restraints listed in Table 2. The observed NOE restraints between the H6, H7, and H8 protons of the AF ring and the base (H8) and sugar (H2′, 2″) protons of dG17 are satisfied in the solution conformation of the adduct duplex (Table 2). This result is consistent with the alignment of the $C^6-C^7-C^8$-containing edge of the AF ring toward the dG17-dG18 segment of the complementary strand in the solution conformation of the [AF]dG·2del 12-mer duplex (Figure 8).

The dG17 imino proton (12.12 ppm) of the dC8·dG17 pair is upfield of the dG18 imino proton (13.17 ppm) of the dC5·dG18 pair in the proton NMR spectrum of the [AF]dG·2del 12-mer duplex (Figure 1A). This reflects the greater stacking of the AF ring with the dC8·dG17 base pair relative to the dC5·dG18 base pair in the solution conformation of the [AF]dG·2del 12-mer duplex (Figure 8A).

The intercalation site is wedge-shaped with the dC5 and dC8 bases of the d(C5-[AF]G6-A7-C8) segment on the modified strand separated by a greater distance than the dG17 and dG18 bases of the d(G17-dG18) segment on the partner strand for the solution conformation of the [AF]dG·2del 12-mer duplex (Figure 8A). The Watson−Crick dC5·dG18 base pair exhibits both a large propeller-twist and buckle in contrast to the normal Watson−Crick dC8·dG17 base pair in the solution conformation of the [AF]dG·2del 12-mer duplex (Figure 8A). A similar distortion was also observed in the adduct duplex containing [AF]dG opposite a −1 deletion (Mao et al., 1995).

Bulge-Induced Helix Bending. There is considerable experimental evidence ranging from NMR (Woodson & Crothers, 1988; Rosen et al., 1992b), fluorescence resonance energy transfer (Gohlke et al., 1994), gel electrophoresis retardation and circularization assays (Rice & Crothers, 1989; Hsieh & Griffith, 1989; Bhattacharyya et al., 1989, 1990; Tang & Draper, 1990; Wang & Griffith, 1991; Lilley, 1995), transient electric birefringence (Zacharias & Hagerman, 1995), and electron microscopy (Wang et al., 1992) that has established bending of DNA at segments containing unopposed bases in the interior of the helix. The extent of bending increases with increasing number of unopposed bases at the bulge site (Hsieh & Griffith, 1989; Gohlke et al., 1994; Zacharias & Hagerman, 1995).

DNA bending has also been reported for other covalent carcinogen adducts positioned opposite deletion sites. These examples range from (+)-*trans-anti*- and (+)-*cis-anti*-benzo[*a*]pyrene-N^2-dG adducts positioned opposite −1 deletion sites (Cosman et al., 1994a,b) to a propano-dG exocyclic adduct positioned opposite a −2 deletion site (Weisenseel et al., 1995) and an [AF]dG adduct positioned opposite a −1 deletion site (Mao et al., 1995).

We detect a bend in the DNA duplex centered about the lesion site in the [AF]dG·2del 12-mer duplex. The bend angle is about 45°, which is in the range for −2 deletions in studies of bend angles as a function of bulge size in unmodified duplexes (Gohlke et al., 1994; Zacharias & Hagerman, 1995). We calculate roll, tilt, and twist angles of 26.6, 26.0, and 17.4°, respectively, between the dC8·dG17 and dC5·dG18 base pairs in the solution structure of the [AF]dG·2del 12-mer duplex [calculated according to the method of Babcock et al. (1993)].

Comparison of [AF]dG Positioned Opposite −1 Deletion and −2 Deletion Sites. We have recently reported on the solution conformations of the [AF]dG adduct positioned opposite a −1 deletion site in the d(C5-[BP]G6-C7)·d(G16-G17) sequence context (Mao et al., 1995). The solution conformations of the central segment of the [AF]dG·1del 11-mer duplex (Mao et al., 1995) and the [AF]dG·2del 12-mer (this study) are shown in the same relative global orientation of the DNA in Figures S2 and 8, respectively.

There are similarities in the structural motifs determined for the [AF]dG·1del (Figure S2A) (Mao et al., 1995) and [AF]dG·2del (Figure 8B) (this study) at the oligomer duplex level. The glycosidic torsion angle of [AF]dG adopts a *syn* conformation in both cases. The aromatic rings intercalate into the helix between flanking dG·dC pairs opposite the deletion site. This is accompanied by displacement of the modified deoxyguanosine into the major groove in the case of [AF]dG opposite a −1 deletion (Figure S2A), while both modified deoxyguanosine and the unpaired 3′-neighboring

deoxyadenosine were displaced into the major groove to form a stacked two-base bulge in the case of the [AF]dG opposite a −2 deletion (Figure 8B).

We observe distinct differences in the stacking pattern of the intercalated AF ring between the dC5·dG17 and dC7·dG16 base pairs for the DNA duplexes containing [AF]dG positioned opposite −2 deletion (this study; Figure 8B) and −1 deletion (Mao et al., 1995; Figure S2B) sites. The intercalated AF ring is displaced toward the minor groove in the [AF]dG·2del 12-mer duplex (Figure 8B), but it is displaced toward the major groove in the [AF]dG·1del 11-mer duplex (Figure S2B). This is reflected in selected differences in aminofluorene proton chemical shifts of the [AF]dG adduct positioned opposite −1 and −2 deletion sites. Thus, the AF(H6) and AF(H7) protons are directly positioned over the purine rings of dG16 and dG17 for the adduct positioned opposite a −1 deletion site (Figure S2B) while they are shifted into the minor groove for the adduct positioned opposite a −2 deletion site (Figure 8B). This overlap alignment readily explains the upfield shifts of the AF(H6) and AF(H7) protons of the [AF]dG adduct positioned opposite the −1 deletion site (squares, Figure 5) relative to the −2 deletion site (circles, Figure 5).

The previous NMR computational conformational study on [AF]dG positioned opposite a −1 deletion site established that the long axis of the intercalated aminofluorene ring is parallel to the long axis of the flanking dG·dC base pairs with the AF ring undergoing 180° flips on the NMR time scale (Mao et al., 1995). Such flips position the C^9-containing edges of the aminofluorene ring alternately in the major (Figure S2B) and minor grooves. By contrast, the current NMR computational study on [AF]dG positioned opposite a −2 deletion site yielded three low-energy conformations that position the C^9-containing edge in the major groove (Figure 7). However, we cannot definitively rule out similar 180° flips of the aminofluorene ring in the case of the [AF]dG·2del 12-mer duplex since the calculations were guided by fewer carcinogen−DNA restraints. There remain discrepancies between the experimental bounds and observed values for the restraints involving the [AF]dG6-(H1′)-AF(H3) and G17(H2′)-AF(H6) proton pairs (Table 2), which could be explained by the alternate conformer.

Comparison of [AF]dG Positioned Opposite a −2 Deletion with Previously Studied Bulged Nucleotides in Solution. Oligonucleotide duplexes containing multiple unpaired bases in various sequence contexts and lengths have been examined previously by NMR (Rosen et al., 1992a,b; Aboul-ela et al., 1993). Rosen et al. (1992a) have shown that one, two, or three unpaired deoxyadenosines in an oligonucleotide adopt an intrahelical conformation, stacking within the duplex in solution as evaluated by NMR spectroscopy. This structural motif has been further illustrated by the solution structure of an oligonucleotide duplex containing a three-base (A-T-A) bulge that established that the unpaired bases retain an *anti* conformation about their glycosidic bonds and stack into the helix (Rosen et al., 1992b).

In addition, solution NMR studies on oligonucleotide duplexes containing an unpaired carcinogen modified base have provided conformational insight into the premutational intermediate that leads to frameshift mutation. Studies on (+)-*trans-anti*- and (+)-*cis-anti*-BPDE-N^2-dG positioned opposite a deletion site have shown that the benzo[*a*]pyrenyl ring is inserted into the helix with the modified deoxyguanosine base in an *anti* conformation and displaced either into the major groove in the case of (+)-*trans-anti*-BPDE adduct (Cosman et al., 1994a) or into the minor groove in the case of (+)-*cis-anti*-BPDE adduct (Cosman et al., 1994b). A more recent study on a (+)-*trans-anti*-BPDE-dG adduct at a single strand−duplex junction which mimics one arm of the replication fork has established that the benzo[*a*]-pyrenyl ring is stacked with the adjacent base pair while the modified deoxyguanosine adopts a *syn* conformation, is displaced into the major groove, and no longer stacks over the adjacent base pair (Cosman et al., 1995). Recent studies on an oligonucleotide containing propanodeoxyguanosine (PdG) positioned opposite a two-base deletion have revealed that PdG adopts an *anti* conformation with respect to the glycosidic bond and that it is intrahelical, while the unpaired 3′-neighboring deoxycytosine adopts a poorly stacked or extrahelical conformation (Moe et al., 1994; Weisenseel et al., 1995). Our previous work on [AF]dG opposite a −1 deletion has demonstrated that the aminofluorene ring is inserted into the helix and that the modified deoxyguanosine adopts a *syn* glycosidic torsion angle and is displaced into the major groove (Mao et al., 1995). The [AF]dG·2del oligonucleotide differs from these in that the [AF]dG forms part of a two-base bulge with its glycosidic torsion angle in the *syn* conformation and looped out of the helix. The two-base bulge is stabilized by the stacking interaction between the extrahelical modified deoxyguanosine and its 3′-neighboring deoxyadenosine which adopts an *anti* conformation about its glycosidic bond. Thus the carcinogen-inserted motif is favorable for polycyclic aromatic or aromatic amine adducts when the modified base is opposite a deletion site or at a single strand−duplex junction irrespective of the specific adduct or linkage site.

Comparison of AF-Modified Oligomer Duplex Solution Conformations. Solution conformations of AF-modified duplexes that have been obtained to date by high-resolution NMR reveal a number of different conformational themes, depending on the sequence context. In normal duplexes with dC opposite the modification site, the AF resides in the B-DNA major groove with the modified deoxyguanosine glycosidic torsion angle in the *anti* domain (Cho et al., 1994; Eckel & Krugh, 1994) in one of two conformers. The second conformer has been identified with AF inserted into the helix with base displacement of the modified base, which is believed to adopt the *anti* conformation (Eckel & Krugh, 1994). When the AF-modified dG is mismatched with dA (Norman et al., 1989) or with dG or dI (Abuaf et al., 1995), AF is sandwiched into the B-DNA minor groove with only its edges exposed and the modified deoxyguanosine glycosidic torsion angle is in the *syn* domain. In the case of the [AF]dG adduct positioned opposite −1 and −2 deletion sites, the modified deoxyguanosine is *syn* and the base displaced while the AF is inserted. Recently, Belguise-Valladier and Fuchs (1995) used chemical probing experiments to show that AF adopts different conformations at dG3 versus dG1 or dG2 in the *Nar*I mutagenesis hotspot d(G1-G2-C-G3-C-C) sequence of *Escherichia coli*. Thus, the context strongly governs the conformation adopted. A context dependent conformational heterogeneity has also been observed for the (+)-*trans-anti*-BPDE-N^2-dG adduct: the carcinogen is in the B-DNA minor groove with *anti*-deoxyguanosine in a normal duplex with dC opposite the lesion (Cosman et al., 1993), in an *anti*-base displaced, carcinogen-inserted conformation

in a −1 deletion context (Cosman et al., 1994), and in a *syn*-base displaced carcinogen-stacked conformation at a single strand−duplex junction that models an arm of a replication fork (Cosman et al., 1995).

Biological Implications. Intercalation of equilibrium bound planar aromatic moieties into DNA helices has long been known to induce frameshift mutations (Streisinger et al., 1966; Drake & Baltz, 1976). The concept of covalent intercalation for a carcinogen-modified base was first proposed by Shapiro and Klein (1967) for β-naphthyl-modified deoxycytidine and subsequently in the base displacement (Grunberger et al., 1970) or insertion−denaturation (Fuchs & Daune, 1973) models for AAF modified deoxyguanosine. That carcinogen−base stacked states may represent mutagenic conformers that are easily accessible from normal base−base stacked structures in DNAs covalently damaged by polycyclic aromatic moieties, including 2-aminofluorene and 2-acetylaminofluorene, was suggested from surveys of the potential energy surface of these adducts by energy minimization (Broyde & Hingerty, 1983, 1984; Hingerty & Broyde, 1986). Recently, Eckel and Krugh (1994) advanced the idea of an AF−base stacked state as an accessible potentially mutagenic conformer in light of their experimental high-resolution NMR study of an [AF]dG-modified duplex with deoxycytidine opposite the modified dG. They find a pair of interconverting conformers with AF in the major groove or inserted into the helix by base displacement of the modified deoxyguanosine. Mechanisms to explain just how planar aromatic moieties might produce frameshift mutations by intercalation have focused on slippage mechanisms, especially in repetitive sequences, since the work of Streisinger (1966) and Drake and Baltz (1976). More recently the concept has been developed further and applied to carcinogen-modified DNAs in a variety of sequence contexts (Schaaper et al., 1990; Kunkel, 1990; Lambert et al., 1992; Shibutani & Grollman, 1993; Napolitano et al., 1994). The essential idea involves stalling of a polymerase in the vicinity of the damaged base, which permits time for a rearrangement in which an unopposed bulge can form. If the bulge is on the damaged template, as in the present work, a deletion results; an insertion would result from a bulge on the newly synthesized partner strand. The marked thermodynamic stabilization observed by us for the [AF]dG·2del 12mer relative to the unmodified analog is in harmony with the notion that a base-displaced, carcinogen-inserted type of structure could account for −2 deletions induced by 2-aminofluorene and perhaps other aromatic amines that link covalently to C^8 of dG. Our previous solution conformation of an [AF]dG-modified duplex with a −1 deletion featured a similar base-displaced AF-inserted conformation (Mao et al., 1995), as did our (+)-*trans-anti*- and (+)-*cis-anti*-BPDE-dG-modified −1 deletion duplex conformations (Cosman et al., 1994a,b). In addition, the recent delineation of a solution conformation of the (+)-*trans-anti*-BPDE-dG adduct at a single strand−duplex junction that models an arm of the replication fork, which features a carcinogen-inserted, base-displaced conformation (Cosman et al., 1995), provides the key experimental structural evidence that conformers of this type are plausible common mutagenic structures at a replication fork in polycyclic aromatic carcinogen adducts irrespective of the specific adduct or linkage site.

The conformation presented in this study is the first experimental molecular view (as far as we are aware) of any carcinogenic polycyclic aromatic amine or hydrocarbon covalent adduct to DNA in a −2 deletion context. Thus, it is important in revealing generically how a polycyclic aromatic amine can stabilize a structure of this type. While −2 deletions are not common in the case of the AF adduct, they are observed (Bichara & Fuchs, 1985). They are profoundly deleterious, as are all frameshifts that induce a change in reading frame, while the point mutations that are more widely observed for AF adducts (Heflich & Neft, 1994) can be benign. Future work should reveal the relationship between the present −2 deletion conformation and −2 deletion conformations in a sequence where such AF-induced mutations are actually observed, such as the *Nar*I sequence of *Escherichia coli* (Bichara & Fuchs, 1985).

SUPPORTING INFORMATION AVAILABLE

Four tables listing exchangeable and nonexchangeable proton chemical shifts for the entire [AF]dG·2del 12-mer adduct duplex, proton chemical shift differences on adduct formation, and backbone torsion angles for the central segment of the energy-minimized conformation of the [AF]dG·2del 12-mer duplex and two figures showing the unrestrained conformations of the entire [AF]dG·2del 12-mer duplex and two views of the central segment of the [AF]dG·1del 11-mer duplex (8 pages). Ordering information is given on any current masthead page.

REFERENCES

Aboul-ela, F., Murchie, A. I. H., Homans, S. W., & Lilley, D. M. J. (1993) *J. Mol. Biol. 229*, 173−188.

Abuaf, P., Hingerty, B. E., Broyde, S., & Grunberger, D. (1995) *Chem. Res. Toxicol. 8*, 369−378.

Arnott, S., Bond, P. J., Selsing, E., & Smith, P. J. (1976) *Nucleic Acids Res. 2*, 2459−2470.

Babcock, M. S., Pednault, E. P. D., & Olson, W. K. (1993) *J. Biomol. Struct. Dyn. 11*, 597−628.

Bax, A., & Subramanian, J. (1986) *J. Magn. Reson. 67*, 565−570.

Beland, F. A., & Kadlubar, F. F. (1990) Chemical Carcinogenesis and Mutagenesis, in *Handbook of Experimental Pharmacology* (Cooper, C. S., & Grover, P. L., Eds.) Vol. 94, Part 1, pp 267−325, Springer-Verlag, Heidelberg.

Belguise-Valladier, P., & Fuchs, R. P. P. (1995) *J. Mol. Biol. 249*, 903−913.

Bhattacharyya, A., & Lilley, D. M. J. (1989) *Nucleic Acids Res. 17*, 6821−6840.

Bhattacharyya, A., Murchie, A. I. H., & Lilley, D. M. J. (1990) *Nature (London) 343*, 484−487.

Bichara, M., & Fuchs, R. P. P. (1985) *J. Mol. Biol. 183*, 341−351.

Broyde, S., & Hingerty, B. E. (1983) *Biopolymers 22*, 2423−2441.

Broyde, S., & Hingerty, B. (1984) *Ann. N. Y. Acad. Sci. 435*, 119−122.

Broyde, S., & Hingerty, B. E. (1987) *Nucleic Acids Res. 16*, 6539−6552.

Carothers, A. M., Urlaub, G., Mucha, J., Yuan, W., Chasin, L. A., & Grunberger, D. (1993) *Carcinogenesis 14*, 2181−2184.

Cho, B. P., Beland, F. A., & Marques, M. M. (1994) *Biochemistry 33*, 1373−1384.

Cosman, M., de los Santos, C., Fiala, R., Hingerty, B. E., Ibanez, V., Luna, E., Harvey, R., Geacintov, N. E., Broyde, S., & Patel, D. J. (1993) *Biochemistry 32*, 4145−4155.

Cosman, M., Fiala, R., Hingerty, B. E., Amin, S., Geacintov, N. E., Broyde, S., & Patel, D. J., (1994a) *Biochemistry 33*, 11507−11517.

Cosman, M., Fiala, R., Hingerty, B. E., Amin, S., Geacintov, N. E., Broyde, S., & Patel, D. J., (1994b) *Biochemistry 33*, 11518−11527.

Cosman, M., Hingerty, B. E., Geacintov, N. E., Broyde, S., & Patel, D. J. (1995) *Biochemistry 34*, 15334−15350.
Drake, J. W., & Baltz, R. W. (1976) *Annu. Rev. Biochem. 45*, 11−37.
Eckel, L. M., & Krugh, T. R. (1994) *Biochemistry 33*, 13611−13624.
Fuchs, K., & Daune, M. (1973) *FEBS Lett. 34*, 295−298.
Garcia, A., Lambert, I. B., & Fuchs, R. P. P. (1993) *Proc. Natl. Acad. Sci. U.S.A. 90*, 5989−5993.
Ghose, R., Marino, J. P., Wiberg, K. B., & Prestegard, J. H. (1994) *J. Am. Chem. Soc. 116*, 8827−8828.
Gohlke, C., Murchie, A. I. H., Lilley, D. M., & Clegg, R. M. (1994) *Proc. Natl. Acad. Sci. U.S.A. 91*, 11660−11664.
Greene, K. L., Wang, Y., & Live, D. (1995) *J. Biomol. NMR 5*, 333−338.
Grunberger, D., Nelson, J. H., Cantor, C. R., & Weinstein, I. B. (1970) *Proc. Natl. Acad. Sci. U.S.A. 66*, 488−494.
Heflich, R. H., & Neft, R. E. (1994) *Mutat. Res.: Rev. Genet. Toxicol. 318*, 73−174.
Hingerty, B. E., & Broyde, S. (1982) *Biochemistry 21*, 3243−3252.
Hingerty, B. E., & Broyde, S. (1986) *J. Biomol. Struct. Dyn. 4*, 365−371.
Hingerty, B. E., Figueroa, S., Hayden, T., & Broyde, S. (1989) *Biopolymers 28*, 1195−1222.
Hsieh, C.-H., & Griffith, J. D. (1989) *Proc. Natl. Acad. Sci. U.S.A. 86*, 4833−4837.
Kraulis, P. J. (1991) *J. Appl. Crystallogr. 24*, 946−950.
Kunkel, T. A. (1990) *Biochemistry 29*, 8003−8011.
Lambert, I. B., Napolitano, R. L., & Fuchs, R. P. P. (1992) *Proc. Natl. Acad. Sci. U.S.A. 89*, 1310−1314.
Lilley, D. M. J. (1995) *Proc. Natl. Acad. Sci. U.S.A. 92*, 7140−7142.
Mah, M. C.-M., Boldt, J., Culp, S. J., Maher, V. M., & McCormick, J. J. (1991) *Proc. Natl. Acad. Sci. U.S.A. 88*, 10193−10197.
Mao, B., Cosman, M., Hingerty, B. E., Broyde, S., & Patel, D. J. (1995) *Biochemistry 34*, 6226−6238.
Melchoir, W. B., Jr., Marques, M. M., & Beland, F. A. (1994) *Carcinogenesis 15*, 889−899.
Michaels, M. L., Reid, T. M., King, C. M., & Romano, L. J. (1991) *Carcinogenesis 12*, 1641−1646.
Moe, J., Reddy, G. R., Marnett, L. J., & Stone, M. P. (1994) *Chem. Res. Toxicol. 7*, 319−328.
Napolitano, R. L., Lambert, I. B., & Fuchs, R. P. P. (1994) *Biochemistry 33*, 1311−1315.
Norman, D., Abuaf, P., Hingerty, B. E., Live, D., Grunberger, D., Broyde, S., & Patel, D. J. (1989) *Biochemistry 28*, 7462−7476.
Patel, D. J., Kozlowski, S. A., Nordheim, A., & Rich, A. (1982) *Proc. Natl. Acad. Sci. U.S.A. 79*, 1413−1417.
Patel, D. J., Shapiro, L., & Hare, D. (1987) *Annu. Rev. Biophys. Biophys. Chem. 16*, 423−454.
Rice, J. A., & Crothers, D. M. (1989) *Biochemistry 28*, 4512−4516.
Rosen, M. A., Live, D., & Patel, D. J. (1992a) *Biochemistry 31*, 4004−4014.
Rosen, M. A., Shapiro, L., & Patel, D. J. (1992b) *Biochemistry 31*, 4015−4026.
Sahm, J., Turkington, E., LaPointe, D., & Strauss, B. (1989) *Biochemistry 28*, 2836−2843.
Schaaper, R. M., Koffel-Schwartz, N., & Fuchs, R. P. (1990) *Carcinogenesis 11*, 1087−1095.
Schlick, T., Hingerty, B. E., Peskin, C. S., Overton, M. L., & Broyde, S. (1990) in *Theoretical Chemistry and Molecular Biophysics* (Beveridge, D., & Lavery, R., Eds.) pp 39−58, Academic Press, New York.
Shapiro, R., & Klein, R. S. (1967) *Biochemistry 6*, 3576−3582.
Shelton, M. L., & DeMarini, D. M. (1995) *Mutat. Res. 327*, 76−95.
Shibutani, S., & Grollman, A. P. (1993) *J. Biol. Chem. 268*, 11703−11710.
Singh, S. B., Hingerty, B. E., Singh, U. C., Greenberg, J. P., Geacintov, N. E., & Broyde, S. (1991) *Cancer Res. 51*, 3482−3492.
Sklenar, V., Miyashiro, H., Zon, G., Miles, H. T., & Bax, A. (1986) *FEBS Lett. 208*, 94−98.
Streisinger, G., Okada, Y., Emrich, J., Newton, J., Tsugita, A., Terzaghi, E., & Inouye, M. (1966) *Cold Spring Harbor Symp. Quant. Biol. 31* 77−84.
Tang, R. S., & Draper, D. E. (1990) *Biochemistry 29*, 5232−5237.
Taylor, E. R., & Olson, W. K. (1983) *Biopolymers 22*, 2667−2702.
Tebbs, R.-S., & Romano, L. J. (1994) *Biochemistry 33*, 8998−9006.
van de Ven, F. J., & Hilbers, C. W. (1988) *Eur. J. Biochem. 178*, 1−38.
Wang, Y. H., & Griffith, J. (1991) *Biochemistry 30*, 1358−1363.
Wang, Y. H., Barker, P., & Griffith, J. (1992) *J. Biol. Chem. 267*, 4911−4915.
Weisenseel, J. P., Moe, J. G., Reddy, G. R., Marnett, L. J., & Stone, M. (1995) *Biochemistry 34*, 50−64.
Woodson, S. A., & Crothers, D. M. (1988) *Biochemistry 27*, 3130−3141.
Ya, N.-Q., Smirnov, S., Cosman, M., Bhanot, S., Ibanez, V., & Geacintov, N. E. (1994) *Structural Biology: The State of the Art*, Proceedings of the Eighth Conversation in the Discipline Biomolecular Stereodynamics, State University of New York at Albany, June 22−26, 1993 (Sarma, R.-H., & Sarma, M., Eds.) Vol. 2, pp 349−366, Adenine Press, Schenectady, NY.
Zacharias, M., & Hagerman, P. J. (1995) *J. Mol. Biol. 247*, 486−500.

BI951595R